*Clays and Clay Minerals*, Vol. 55, No. 3, 295–310, 2007.

# ALTERATION OF SPODUMENE TO COOKEITE AND ITS PRESSURE AND TEMPERATURE STABILITY CONDITIONS IN Li-BEARING APLITE-PEGMATITES FROM NORTHERN PORTUGAL

IULIU BOBOS[1,*], PHILIPPE VIEILLARD[2], BERNARD CHAROY[3] AND FERNANDO NORONHA[1]

[1] GIMEF-Departamento de Geologia, Faculdade de Ciências, Universidade do Porto, Rua do Campo Alegre 687, P-4169-007 Porto, Portugal
[2] UMR-CNRS 6532 HYDRASA, 40 avenue du Recteur Pineau, Université de Poitiers, F-86022 Poitiers Cedex, France
[3]CRPG-CNRS, Ecole Normale Supérieure de Géologie, F-54501 Vandœuvre-lès-Nancy Cedex, France

**Abstract**—The alteration of spodumene to cookeite has been identified in a Li-bearing aplite-pegmatite from northern Portugal. Optical microscopy and scanning and transmission electron microscopy (SEM/TEM) were used to characterize the alteration products in both cookeite + quartz and cookeite + kaolinite ± mica assemblages. Mutual relationships between the minerals were assessed using back-scattered electron imaging. The first assemblage occurs along the cleavage planes of spodumene, whereas the second forms as the result of spodumene breakdown. Fine mica grains surrounded the cookeite aggregates in the second assemblage only. Precipitations of cookeite and quartz in open pore spaces and parallel packets of cookeite and kaolinite were identified by TEM. Selected area electron diffraction carried out on cookeite identified a layer-stacking sequence from highly disordered to one-layer order-disorder with a lesser participation of two-layer polytypes. The thickness of one-layer cookeite packets averaged ~85−100 nm. Disordered cookeite has a mean thickness of 450 nm. The chemistry of cookeite was analyzed by both electron and ion-microprobe techniques. The structural formula of cookeite from the first assemblage corresponds to: $Al_{2.0}(Si_{3.23}Al_{0.766})O_{10}(OH)_2(Al_{1.80}Li_{1.166}Mg_{0.004}Fe_{0.09})(OH)_6$. Two distinct compositional varieties were found: one corresponding to ideal cookeite, whereas the second belongs to the cookeite–donbassite join.

The thermodynamic stability field for the observed minerals was calculated using the SUPCRT® programme. Two distinct stages of cookeite crystallization are discussed. The lower pressure and temperature stability of the reaction of spodumene to cookeite + quartz were estimated at ~2.4 kbar and 240ºC. The cookeite + kaolinite ± mica assemblage is still in equilibrium with quartz at ~2.2 kbar and 220ºC. The lower limit for the stability of cookeite was found at 205ºC and 2 kbar.

**Key Words**—Cookeite, Crystal Chemistry, Electron Microscopy, Kaolinite, Polytype, Spodumene Breakdown, Thermodynamic Stability.

## INTRODUCTION

The widespread hydrothermal alteration of anhydrous lithium (Li) aluminosilicates (*i.e.* spodumene, petalite, eucryptite, lepidolite, elbaite, *etc.*) to a variety of secondary mineral phases or assemblages including albite, K-feldspar, muscovite, cookeite, kaolinite and montmorillonite, is well known (Černý, 1970, 1972; London and Burt, 1982; Foord *et al.*, 1986; Wood and Williams-Johns, 1993; Singh and Gilkes, 1993). Spodumene alteration to petalite + eucryptite and/or albite + micas in granitic pegmatites is associated with an initial stage involving sub-solidus reactions of the lithium minerals (London and Burt, 1982; Charoy *et al.*, 2001), followed by an alkaline metasomatic stage characteristic of closed-system pegmatite evolution (Wood and Williams-Johns, 1993). Thus, the presence of micas or other phyllosillicates related to spodumene alteration reflects changes from neutral to relatively acidic environments (Hemley and Johns, 1964), suggesting an open-system evolution that allows for argillic wall-rock alteration.

Cookeite, a Li di,trioctahedral chlorite, was first identified as a late-stage hydrothermal alteration product in pegmatitic environments at Maine (Penfield, 1894) and at Castelnau de Brassac (Arsandaux, 1901; Lacroix, 1915). Since then, cookeite has been described in several pegmatite fields around the world (Quensel, 1937, 1956; Pecora *et al.*, 1950; Hensen, 1967). It occurs as an alteration of either rubellite, spodumene (Lacroix, 1915; Černý *et al.*, 1971; Foord *et al.*, 1986) or even lepidolite (Černý, 1970; Foord *et al.*, 1986). In the Tanco pegmatite, cookeite was found associated with adularia, quartz, zeolites and carbonates as fracture-controlled replacements of spodumene and petalite (Heinrich, 1975). Cookeite, pollucite and albite were also identified in fluid inclusions in spodumene pegmatites from Kulam, Afghanistan (London, 1986).

Despite the abundance of Li-rich layer silicate alteration products in pegmatites, B-rich or B-bearing cookeite occurs only scarcely in nature. Several occurrences are known from Muiane, Mozambique (Sahama *et al.*, 1968), Radkovice, Czech Republic (Černý *et al.*, 1971) and Malkhan, Russia (Zagorsky *et al.*, 2003).

* E-mail address of corresponding author:
ibobos@fc.up.pt
DOI: 10.1346/CCMN.2007.0550306

Besides occurring in pegmatitic environments, cookeite was also found associated with rectorite + quartz assemblages (Miser and Milton, 1964) in hydrothermal quartz veins (Stone and Milton, 1976), as well as in pyrophyllite (Orliac *et al.*, 1971) and diaspore (Loughnan and Steggles, 1976) occurrences, antimony veins (Shimada *et al.*, 1985), and quartz, cassiterite and topaz assemblages (Ren *et al.*, 1988).

Therefore, cookeite is known to occur in various geological environments such as: diagenetic (Flehmig and Menschel, 1972), low-grade, low-pressure metamorphic schists (Fischer *et al.*, 1989); medium-grade, low-pressure metabauxites (Sartori, 1988); low-grade, high-pressure metapelites and metabauxites (Goffé, 1977; Goffé *et al.*, 1994; 1996); as well as in high-pressure and high-temperature conditions (Theye *et al.*, 1992). Hence, we can conclude that cookeite forms commonly in Li-bearing rock systems in diagenetic, metamorphic and hydrothermal environments.

The stability field of cookeite extends over a variety of pressures, from 1 to 14 kbar, and within a narrow temperature range, from 260 to 480ºC (Vidal and Goffé, 1991). Thus, cookeite polytypes have been proposed as geobarometers (Jullien *et al.*, 1996). Nevertheless, the validity of ordered cookeite polytypes as low- to high-pressure indicators was seriously questioned by Mata *et al.* (2004)

The present study discusses textural, mineralogical and crystal chemistry characteristics of the spodumene to cookeite alteration process. It also advances the knowledge of the relative pressure and temperature stability fields of spodumene and cookeite, and it contributes to an understanding of hydrothermal processes in the Li-bearing aplite-pegmatite from northern Portugal.

## GEOLOGICAL BACKGROUND

Aplite-pegmatite dikes hosted by Silurian low- to medium-grade metasedimentary rocks occur in northern Portugal (Figure 1), within the Middle Galicia Tras-os-Montes geotectonic zone (Julivert *et al.*, 1974). Three Hercynian deformation phases (D1 to D3) expressed by three superimposed schistosities (S1 to S3) were recognized by Noronha *et al.* (1981). Several granite bodies with variable mineralogy (biotite or two-mica) and degrees of deformation, occur close to the pegmatite belt.

Two types of aplite-pegmatite dikes were found in northern Portugal (Charoy *et al.*, 1992). The first type consists only of aplite dikes and veins associated with Sn mineralization, whereas the second type includes larger aplite-pegmatitic dikes with spodumene, which are unevenly distributed.

The aplite-pegmatite dikes display irregular patterns in outcrop: some are flat-lying, others have gentle or steep dips along strike. For both types, the wider dikes pinch and swell in accordance with the ductility of their host rocks. Most of these dikes seem to be fracture controlled, suggestive of pegmatite-forming magmas ascending along dilation zones or structural planes in enclosing schists during and after peak metamorphism (Brisbin, 1986). Irregularities (branching or bulging) of dike shapes may result from irregularities in the fracture system. Dike orientation is mainly controlled by S2 foliation, locally deformed by S3 features (crenulations with sub-vertical axial planes striking roughly N120ºE).

The internal structure of the dikes is difficult to assess in the field due to outcrop weathering. However, the dikes have mixed aplitic-granular pegmatitic textural

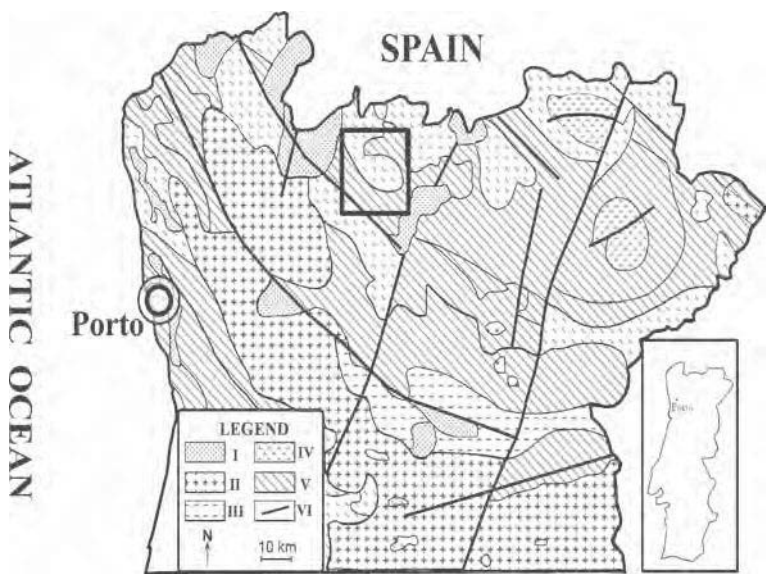


Figure 1. Geological map of northern Portugal (after Ferreira *et al.*, 1987). Legend: I – post-tectonic (post-$D_3$) biotite granites; II – late-tectonic biotite granites; III – syn-tectonic two-mica granites; IV – ultrabasic complex of Bragança-Morais; V – metasedimentary rocks; VI – shear zones and faults. The square indicates the locations of the aplite-pegmatite field.

https://doi.org/10.1346/CCMN.2007.0550306 Published online by Cambridge University Press

components. Because the two textures mix in variable proportions and have varied spatial relationships, they were probably contemporaneous.

## MATERIALS AND METHODS

Samples of spodumene altering to cookeite from the aplite-pegmatite dikes were identified by optical microscopy. Carbon-coated polished thin-sections were investigated by electron microprobe analysis (EMPA) with a Cameca SX50 microprobe equipped with an energy-dispersive X-ray (EDX) analyzer. Electron microprobe analyses were carried out following Velde's (1984) recommendations in order to prevent alkali loss and clay mineral breakdown. Analytical conditions were as follows: accelerating voltage – 15 kV, beam current – 20 nA, peak counting time – 20 s. The standards were albite for Na, magnesite for Mg and orthoclase for Al, Si and K. Lithium was analyzed by ion microprobe (Cameca 3f). Polished samples were coated with gold and sputtered by an $O^-$ primary ion beam of 0.5 to 2.5 nA intensity, 10 keV energy, and focused to $\leqslant$10 μm diameter. The secondary positive ions were accelerated at 4.5 keV and only high-energy secondary ions signals were analyzed. The $^{6}$Li, $^{7}$Li, $^{28}$Si and $^{30}$Si isotopes were measured.

Back scattered and secondary electron microscopy observations were carried out on a JEOL JSM-6000 scanning electron microscope. The samples were crushed in fresh or porous surface pieces, cleaned ultrasonically and then carbon coated.

Representative areas where spodumene had altered to cookeite, as seen by optical microscopy, were selected for the TEM work. A Philips CM-20 transmission electron microscope equipped with an ultrathin window energy dispersive X-ray spectrometer (EDS) working at 120 kV was used to examine ion-thinned samples. The chemistry of cookeite single crystals was determined qualitatively by analytical electron microscopy (AEM).

## RESULTS

### *Optical microscopy and back-scattered electron microscopy (BSEM)*

Cookeite aggregates were observed, using optical microscopy, along fractures or within the cleavage planes of spodumene and commonly, as fine-grained radial aggregates or rosettes replacing spodumene. Radial clusters of cookeite were also present within spodumene aggregates. Cookeite is a low birefringence mineral, with oblique extinction, negative elongation, and first-order grey to light yellow and blue interference colors.

Several mutual relationships between cookeite and its associated minerals were observed in BS-SEM. Along spodumene cleavage planes, cookeite occurs in assemblage with quartz (Figure 2a). Cookeite and quartz assemblages commonly fill cleavage fractures in spodumene. Cleaved regions of spodumene have been widened by dissolution, and the coarse-grained cookeite and quartz alternate rhythmically within the 20 to 600 μm thick spaces. No phases other than cookeite and quartz were observed within the enlarged cleavages. Such observations reflect the scale of local micro-environmental control of the spodumene alteration.

When spodumene has completely altered, it is replaced by an assemblage of cookeite and kaolinite (identified by TEM) (Figure 2b). The pseudomorphic

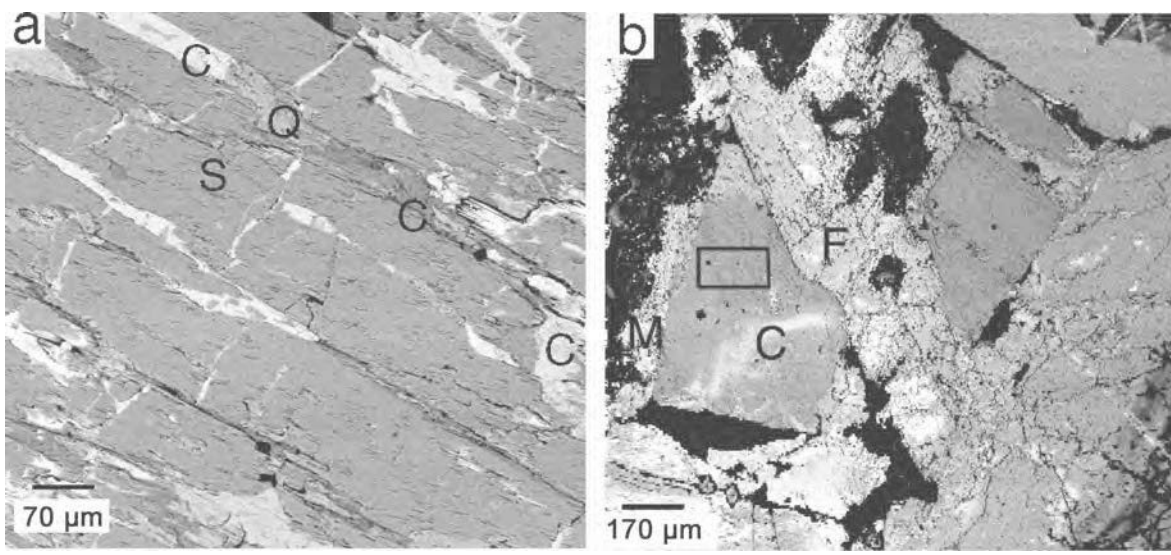


Figure 2. BSEM images of the cookeite (C) and quartz (Q) assemblage coexisting with spodumene (a). Spodumene is substituted by the assemblage of cookeite and kaolinite. K-feldspar (F) occurs at the contact with the finest grains of mica (M) and cookeite (b). The square shows the area investigated.

https://doi.org/10.1346/CCMN.2007.0550306 Published online by Cambridge University Press

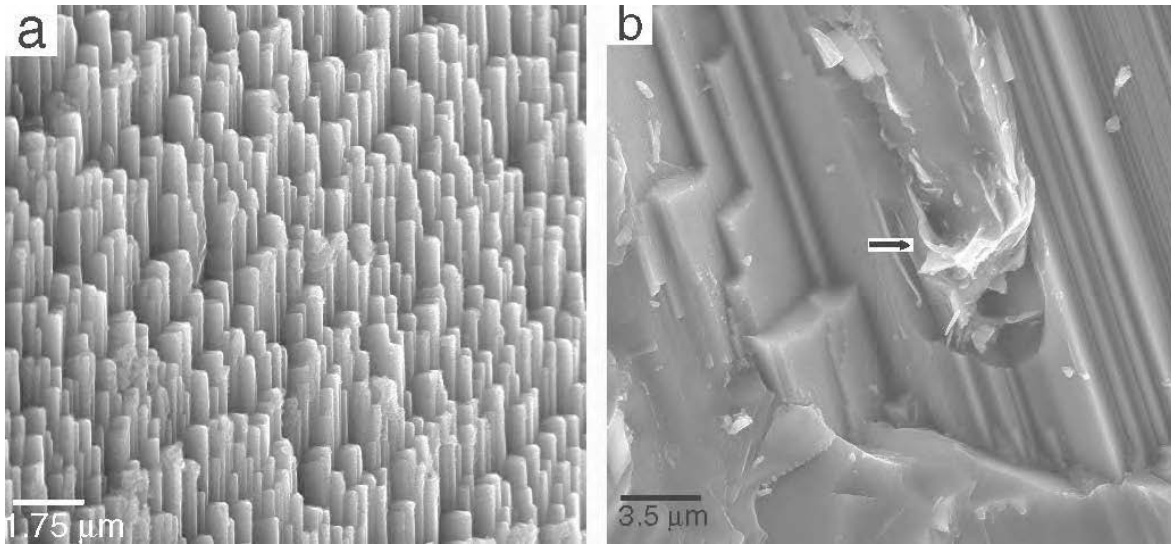


Figure 3. SEM image of spodumene crystals showing columnar habit (a). Dissolution of spodumene and growth of the clay layers in cavities is indicated by an arrow (b).

replacement of spodumene by large masses of cookeite occurs without quartz precipitation. Tapered aggregates of cookeite range in size from 500 µm to 1–1.5 mm as shown in Figure 2b. These cookeite aggregates are surrounded by the mica grains, which are also occasionally in contact with K-feldspar. Mica grains are absent along the cleavage planes of spodumene.

*Scanning electron microscopy*

Spodumene crystal morphology and the relationship with its alteration products were investigated by SEM. Fresh spodumene crystals have a columnar shape suggestive of coalescence growth. The crystals show a common or 'coherent' orientation probably due to a shared nucleation substrate (Figure 3a). Large grains were covered by a myriad of individual spodumene crystals. Rough surface-leached layers resulting from spodumene dissolution and porous hydrated layers on the dissolved spodumene surface were observed on a micrometer scale. The surface dislocations and fractures of spodumene crystals are sites of excess energy where the mineral dissolves much more readily, and they may act as nucleation points. This interpretation is supported by the presence of cookeite packets confined to spodumene dissolution cavities (Figure 3b).

*Transmission electron microscopy*

*Cookeite + quartz assemblage*. The TEM observations of ion-milled sections revealed randomly oriented cookeite packets and some authigenic quartz grains in open cavities (Figure 4). The consequence of open space formation at mineral surfaces is attributed to the nature of interactions between minerals and fluids by reducing atomic-scale porosity at reaction fronts. Lenticular pores and irregularly shaped cavities between stacks of clay particles are observed, where quartz grains fill the abundant pore spaces between the clay packets. Well defined individual parallel and sub-parallel packets of cookeite with thicknesses ranging between ~80 and

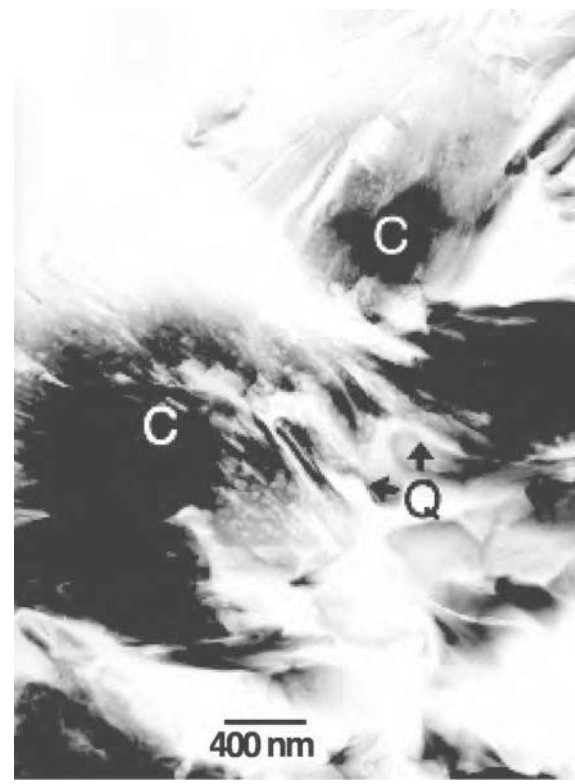


Figure 4. Textural relationship between cookeite (C) and authigenic quartz (Q) observed by TEM.

https://doi.org/10.1346/CCMN.2007.0550306 Published online by Cambridge University Press

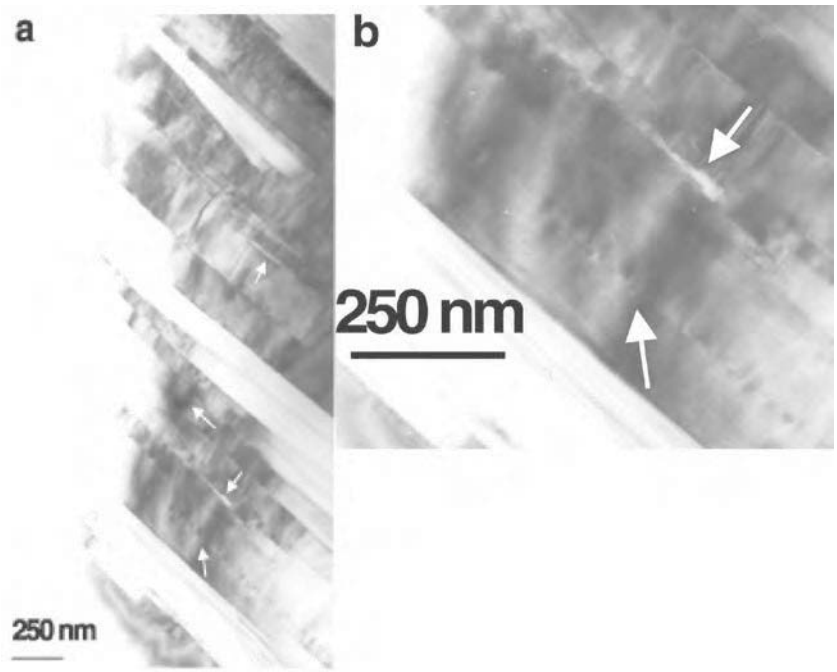


Figure 5. TEM images of (a) cookeite packets with sharp boundaries, dislocations and defects marked by arrows; (b) structural defects and dislocations caused by gliding along the (001) plane highlighted by arrows.

300 nm were observed (Figure 5a). Minimal differences in the thickness of packets and no layer terminations are noted. The largest dimension of the cookeite packets is ~1400 nm. No strain contrast at the packet edge was observed, suggesting no structural misfit. Packets comprising only cookeite have sharp boundaries defined by a continuous (001) layer (Figure 5a). Figure 5b shows a number of defects in adjacent cookeite packets and dislocations in the (001) plane, which are commonly associated with linear features caused by gliding along the (001) plane. The strain fields of the dislocations are also visible as regions with high contrast parallel to the (001) plane.

Figure 6a shows a lattice-fringe image of cookeite crystallites displaying a variety of planar defects along 001. The layer thickness of individual crystals is 85–100 nm. Distinct lenses of 2 to 6 layers were also observed. At high magnification the crystal displays (001) lattice-fringe images with a 1.4 nm periodicity (Figure 6b). A crystal composed of 18 layers (25.2 nm thick) is shown in the upper part of figure, and a number of layer termination defects are marked by white arrows.

A selected area electron diffraction (SAED) study was conducted by systematically orienting cookeite crystals along *hkl* diffraction rows, in order to determine the degree of disorder in the crystals. Representative SAED patterns of cookeite single crystals recorded along [100] reveal a disordered or a semi-random stacking structure in their stacking sequences parallel to $c^*$ in $k \neq 3n$ diffraction rows. The short-period 1L (one-layer) polytype is characterized by diffuse intensity modulations and weak streaking that links 1L spots, whereas diffuse intensity spots with maxima at half of the 1L reciprocal spacing characterizes the 2L (two-layer) stacking sequences. The presence of very diffuse lattice fringes of 1L cookeite with a high degree of disorder could be inferred by SAED (Figure 7a). Also, a 2L periodicity is superimposed on streaks parallel to $c^*$ in $k \neq 3n$ reflections (Figure 7b). The diffraction pattern indicates slightly disordered 2L cookeite as an integrally intergrown structure within 1L cookeite, which was found in crystals >25 nm thick. Therefore, the disorder increases as thickness increases.

*Cookeite + kaolinite assemblage*. A representative low-magnification TEM image of parallel packets of cookeite and kaolinite (marked by arrow) is shown in Figure 8. Both cookeite and kaolinite packets were identified as being at the expense of spodumene alteration (Figure 2b). No lateral transition between kaolinite and cookeite was observed. Thus, no 7 Å layers within 14 Å layers, or *vice versa*, were recognized. Kaolinite, like berthierine, has $d_{001}$ ~7 Å and these phases are distinguished from each other only with difficulty. Under TEM, kaolinite layers show a great instability at higher magnification and are rapidly damaged in part by dehydration in vacuum or by interaction with the electron beam. Structural damage is revealed by contrast zones. Defects and dislocations were not seen in cookeite packets. The size of the packets and structural disorder of cookeite in this assemblage are greater than those observed in the cookeite + quartz assemblage. The thickness of the cookeite packets range from 400 to 450 nm, whereas the

https://doi.org/10.1346/CCMN.2007.0550306 Published online by Cambridge University Press

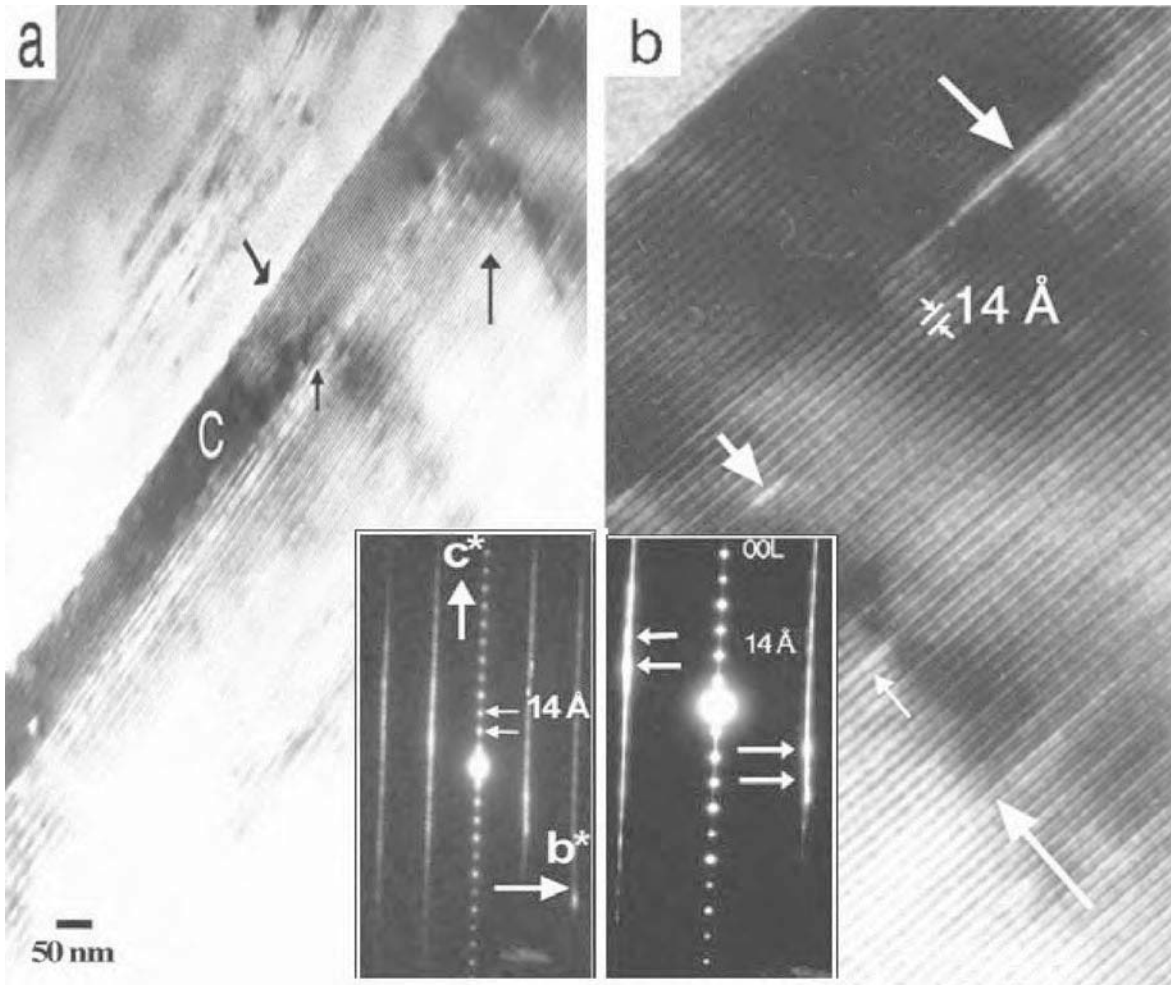


Figure 6. TEM image of cookeite (C) packets and the corresponding SAED pattern indicating a 1L disorder structure (a). High-magnification TEM lattice-fringe image of cookeite crystals and SAED pattern show distinct 1L disorder with modulations (b). Defects at the crystallite boundary or in the middle of packets are marked by arrows.

thickness of the kaolinite packets is ~100–130 nm. The SAED patterns of cookeite show a highly disordered structure (Figure 8).

*Crystal chemistry*

The cookeite structure is characterized by dioctahedral 2:1 layers alternating with trioctahedral hydroxide sheets. The total octahedral occupancy ranges from 4.8 to 5.3 atoms per 6.0 sites; $Li^+$ content ranges from 0.8 to 1.4 a.p.f.u. Lithium was assumed to occur in the brucitic sheet. Tetrahedral aluminum ($^{IV}Al$) is always close to 1.0 atoms per 4.0 tetrahedral sites; occasionally $^{IV}Al$ may be replaced by small amounts of B or Be (Černý, 1970). The theoretical composition of cookeite is $Al_2(Si_3Al)O_{10}(OH)_2(Al_2Li)(OH)$.

Electron microprobe analyses were carried out on cookeite from both assemblages. The fields of cookeite analyzed are shown in Figure 2a,b. The structural formulae of the cookeite specimens analyzed (calculated on a base of 14 oxygens) are given in Table 1. The chemical data obtained were compared with cookeite analyses from a few other pegmatite occurrences. The sum of octahedral cation occupancy per half unit ranges from 4.53 to 5.06. The $Li^+$ content is found to be greater in cookeite from the cookeite + quartz assemblage. Lithium is assumed to replace either $Mg^{2+}$ or $Fe^{2+}$ in the octahedral sheet; a poor correlation, however, was found between $Li^+$ and $R^{2+}$. The amount of Fe decreases as $Li^+$ increases in only one sample (C5). Because $Mg^{2+}$ is in very short supply in the analyzed sample, the oxidation of Fe may provide an alternative means for charge balance. The presence of small amounts of $Fe^{2+}$ and $Mg^{2+}$ was interpreted to indicate a minor miscibility of cookeite for sudoite (Goffé *et al.*, 1996**).**

Spodumene, petalite, eucryptite, bikitaite, cookeite and kaolinite compositions were plotted in the Li-Si-Al ternary diagram (Figure 9). The spodumene and petalite compositions are from Charoy *et al.* (1992), whereas those of eucryptite and bikitaite are after London and Burt (1982). The kaolinite field corresponds to an ideal

https://doi.org/10.1346/CCMN.2007.0550306 Published online by Cambridge University Press

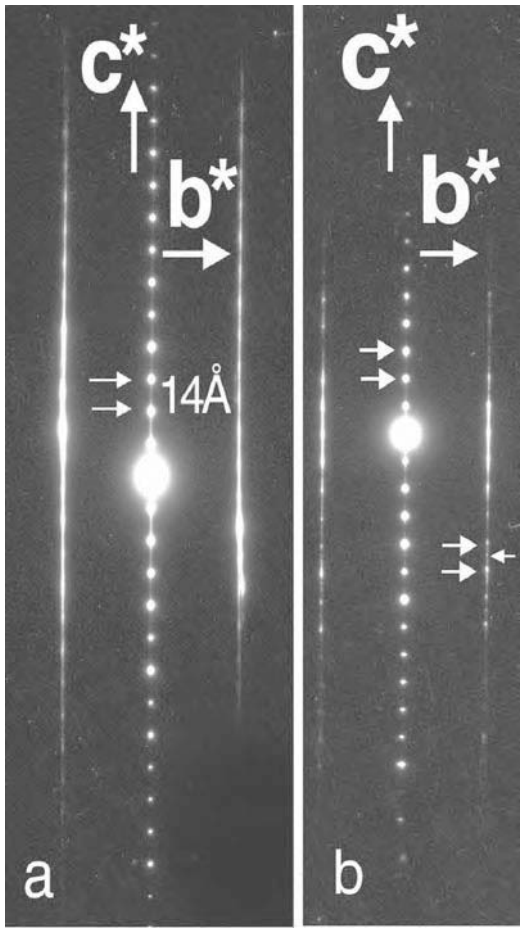


Figure 7. SAED patterns of cookeite crystals recorded along [100] with streaking parallel to $c^*$ in $k\,3n$ diffraction rows. 1L polytype with disorder and modulations (a); and integral dominant 1L and slight 2L disorder (b).

composition (Si/Al $\approx$ 1). The spodumene and eucryptite fields are closely related, whereas the field corresponding to petalite is far from the spodumene field. The compositional field of pegmatitic cookeite is close to that of metamorphic cookeite. The reaction path is indicated by arrows.

Pegmatitic cookeite from Dobra Voda (Černý, 1970), Varuträsk (Quensel, 1956) and Zambezia (Sahama *et al.*, 1968) fall outside the ideal cookeite field in the diagram of total octahedral content *vs*. $Li_2O$ (wt.%) (Figure 10); our samples and the metamorphic cookeite of Jullien *et al.* (1996) are distributed along the cookeite–donbassite joins. Two cookeite samples (C2 and M) show a small deviation from the cookeite–donbassite joins, because the samples contain more Fe (C2) and Mg (metamorphic cookeite from Tzigarine).

The octahedral cation occupancy of pegmatitic cookeite from northern Portugal (Table 1) was plotted in the $^{VI}$Al-(Mg + Fe)-Li diagram (Figure 11) and then compared with octahedral cation distributions in sudoite (Bailey and Lister, 1989), tosudite (Ichikawa and Shimoda, 1976) and donbassite (Merceron *et al.*, 1988). Based on this diagram, an intermediate composition between donbassite and theoretical cookeite characterizes the pegmatitic and metamorphic cookeite.

*Pressure and temperature conditions of the alteration of spodumene to cookeite*

To evaluate the pressure and temperature conditions under which the hydrothermal alteration of spodumene took place, we consider the $LiAlSiO_4$-$SiO_2$-$H_2O$ ternary system (London, 1984; Vidal and Goffé, 1991). The system contains the following minerals identified in the investigated samples: spodumene-petalite-eucryptite-microcline-cookeite-quartz-kaolinite-muscovite-diaspore. Thermodynamic data for these minerals are shown in Table 2. The thermodynamic solubilities for the system were calculated using the SUPCRT® programme (Johnson *et al.*, 1992).

Six variables were chosen for the system: pressure, temperature, pH and the activities of $Li^+$ ($a_{Li^+}$), $K^+$ ($a_{K^+}$) and $SiO_2$ ($a_{SiO_2}$). The activity diagrams were calculated assuming constant Al in the entire system. The stability fields for Li-bearing minerals are represented in two parts: a diagram of log ($a_{Li^+}$) + pH *vs.* log ($a_{SiO_2}$) (Figure 12) and a diagram of log ($a_{Li^+}$) + pH *vs.* log ($a_{K^+}$) + pH (Figure 13). We calculated stability relations for four sets of pressure-temperature values ranging from 2.6 kbar and 260ºC down to 2.2 kbar and 220ºC, in order to establish the lower stability limit for cookeite. The dotted line (Figure 12) corresponds to the equilibrium of the fluid with quartz, and helps to fix the activity of silica in our calculations. When pressure and temperature decrease, the stability field of the cookeite diminishes and its equilibrium boundaries with spodumene, eucryptite, muscovite and kaolinite move towards low values of log ($a_{K^+}$) + pH and log ($a_{SiO_2}$) and towards high values of log ($a_{Li^+}$) + pH. It was assumed that for each of the four calculated pressure and temperature conditions, the chemical composition of the fluids is on the equilibrium line and only two degrees of freedom are present corresponding to log ($a_{Li^+}$) + pH and log ($a_{K^+}$) + pH. For each of the four sets of pressure and temperature conditions, the hypothetical chemical fluid is represented by points from A to D (Figures 12 and 13). The positions of the four points are arbitrary choices.

With respect to silica, the ratio of log ($a_{Li^+}$) + pH and log ($a_{K^+}$) + pH diminishes with decreasing pressure and temperature. However, the rate of the decrease depends upon the decrease in the activities of $Li^+$ and $K^+$. Accordingly, four paths are considered:

large decrease of log ($a_{Li^+}$) + pH with small decrease of log ($a_{K^+}$) + pH;
small decrease of log ($a_{Li^+}$) + pH with large decrease of log ($a_{K^+}$) + pH;
large decrease for log ($a_{Li^+}$) + pH and log ($a_{K^+}$) + pH;
small decrease for log ($a_{Li^+}$) + pH and log ($a_{K^+}$) + pH.

https://doi.org/10.1346/CCMN.2007.0550306 Published online by Cambridge University Press

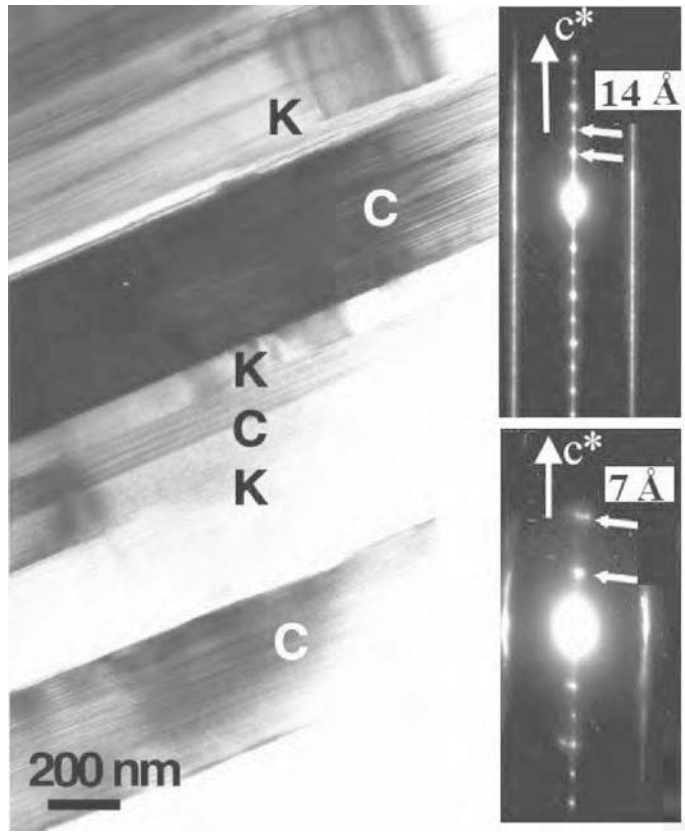


Figure 8. Representative low-magnification TEM image of the intergrowth of cookeite (C) and kaolinite (K) packets. SAED patterns of highly disordered structures of cookeite and kaolinite are shown on the right.

Table 1. Structural formulae of the pegmatitic cookeite samples analyzed.

| Cations | C1 $n$ = 7 | C2 n = 7 | C3 $n$ = 7 | C4 $n$ = 7 | C5 $n$ = 7 | Dobra[1] | Tarn[2] | Zambezia[3] | Varuträsk[4] |
|---|---|---|---|---|---|---|---|---|---|
| Si | 3.21 | 3.31 | 3.19 | 3.24 | 3.23 | 3.06 | 3.27 | 3.24 | 3.29 |
| Al | 0.79 | 0.69 | 0.81 | 0.76 | 0.77 | 0.94 | 0.73 | 0.76 | 0.71 |
| ΣTet. | 4.00 | 4.00 | 4.00 | 4.00 | 4.00 | 4.00 | 4.00 | 4.00 | 4.00 |
| Charge | −0.79 | −0.69 | −0.81 | −0.76 | −0.77 | −0.94 | −0.73 | −0.76 | −0.71 |
| Al | 3.89 | 3.87 | 3.87 | 3.87 | 3.80 | 3.82 | 3.90 | 3.97 | 3.68 |
| $Fe^{2+}$ | 0.14 | 0.18 | 0.11 | 0.14 | 0.09 | 0.00 | 0.00 | 0.00 | 0.11 |
| Mn | 0.00 | 0.00 | 0.00 | 0.00 | 0.00 | 0.00 | 0.00 | 0.00 | 0.00 |
| Mg | 0.00 | 0.00 | 0.01 | 0.01 | 0.00 | 0.00 | 0.00 | 0.00 | 0.005 |
| Li | 0.82 | 0.69 | 0.46 | 0.82 | 1.17 | 1.46 | – | 1.11 | 1.53 |
| ΣOct. | 4.85 | 4.74 | 4.45 | 4.84 | 5.06 | 5.29 | – | 5.08 | 5.30 |
| Charge | 0.77 | 0.66 | 0.31 | 0.73 | 0.75 | 0.92 | – | 0.81 | – |
| Ca | 0.00 | 0.00 | 0.00 | 0.00 | 0.00 | 0.00 | 0.00 | 0.01 | 0.03 |
| Na | 0.00 | 0.00 | 0.01 | 0.01 | 0.01 | 0.01 | 0.00 | 0.01 | 0.00 |
| K | 0.01 | 0.01 | 0.01 | 0.01 | 0.01 | 0.01 | 0.00 | 0.00 | 0.05 |
| Total charge | −0.01 | −0.02 | −0.48 | −0.01 | 0.00 | 0.00 | – | 0.07 | – |
| $R^{++}$ | 0.14 | 0.18 | 0.12 | 0.15 | 0.09 | 0.00 | 0.00 | 0.00 | 0.00 |
| $R^{+}$ | 0.01 | 0.01 | 0.02 | 0.02 | 0.02 | 0.02 | 0.01 | 0.02 | 0.00 |

C1, C2, C3: cookeite + kaolinite assemblage; C4, C5: cookeite + quartz assemblage
[1] Černý *et al.* (1971); [2] Jullien *et al.* (1996); [3] Sahama *et al.* (1976); [4] Quensel (1956).
$n$ = number of analyses.

https://doi.org/10.1346/CCMN.2007.0550306 Published online by Cambridge University Press

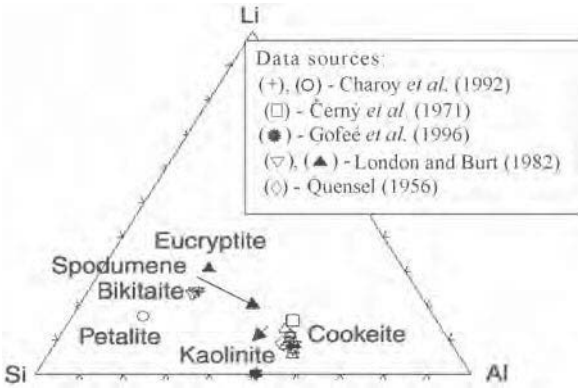


Figure 9. A synthetic plot in the Li-Si-Al ternary system of the chemical composition of spodumene (+), petalite (○), bikitaite (▽), eucryptite (▲), kaolinite (★), pegmatitic cookeite from Dobra (□), Varuträsk (◇), Portugal (△) and metamorphic cookeite (✻) reported in the literature. The starting reaction is from spodumene to cookeite indicated by the arrow.

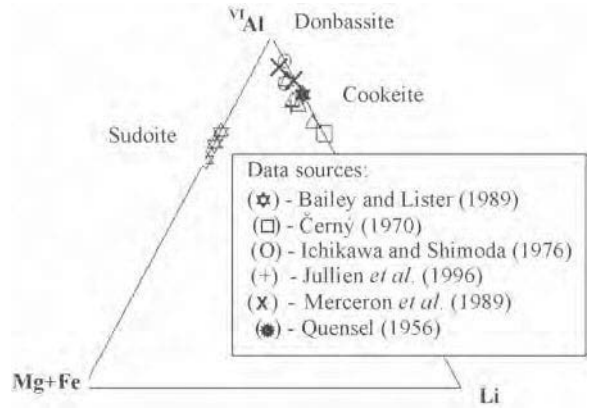


Figure 11. Octahedral cations of pegmatitic cookeite from Portugal (△), Dobra (□), Varuträsk (★), metamorphic cookeite (+), sudoite (✡), donbassite (X) and tosudite (○) plotted in the Li-(Mg + Fe)-$^{VI}$Al diagram.

Each of these four paths is delimited by a small box characterizing the limits of values of log ($a_{Li^+}$) + pH, log ($a_{K^+}$) + pH, and log$(SiO_2)_{aq}$.

(a) Set 1: $P$ = 2.6 kbar, $T$ = 260ºC;

The fluid (point A in Figures 12 and 13) is assumed to be in equilibrium with respect to the quartz + spodumene assemblage.

(b) Set 2: $P$ = 2.4 kbar, $T$ = 240ºC;

When both pressure and temperature decrease, point A moves to B, and appears on the cookeite–spodumene equilibrium line and on the boundary between $SiO_2$(aq) and quartz (Figure 12). These compositional parameters signify the lowest limit of the transformation of spodumene to cookeite + quartz.

The cookeite-to-muscovite reaction may be controlled by the value of log ($a_{K^+}$) + pH (Figure 13). When log ($a_{K^+}$) + pH of the fluid increases, point B moves towards the muscovite−cookeite equilibrium line and muscovite formation is favored. In addition, the decrease of pressure and temperature at constant values of log ($a_{K^+}$) + pH and log ($a_{Li^+}$) + pH can promote the transformation of cookeite to muscovite.

(c) Set 3: $P$ = 2.3 kbar and $T$ = 230ºC.

Point B moves to point C when pressure and temperature decrease (Figures 12 and 13). Point C corresponds to the equilibrium of the solution with respect to quartz, cookeite and muscovite. Under these conditions, spodumene has been completely replaced and there is no production of cookeite by spodumene alteration (for solutions in equilibrium with quartz). Cookeite can still remain stable or could be transformed into muscovite, even for pressure and temperature values slightly below 2.3 kbar and 230ºC.

(d) Set 4: $P$ = 2.2 kbar and $T$ = 220ºC.

When pressure and temperature decrease to 2.2 kbar and 220ºC, point C moves to point D (Figures 12 and 13) and the system is still in equilibrium with quartz. The

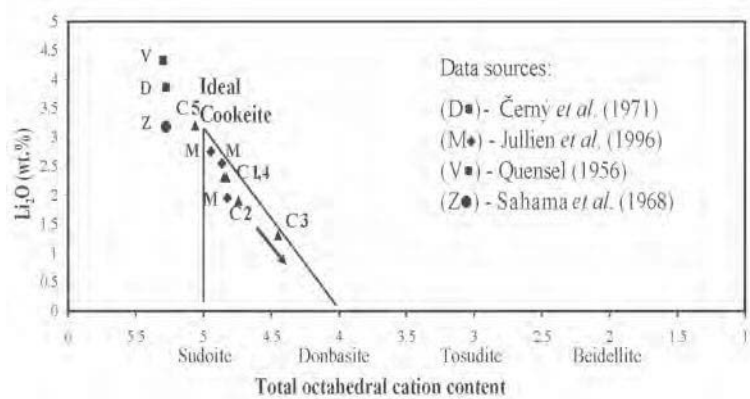


Figure 10. The relationship between $Li_2O$ (wt.%) and total octahedral content per half unit-cell. Pegmatitic cookeite from Portugal (C) and metamorphic cookeite (M) are plotted along the cookeite−donbassite joins.

https://doi.org/10.1346/CCMN.2007.0550306 Published online by Cambridge University Press

Table 2. Thermodynamic data (enthalpy, Gibbs free energies of formation, entropy, heat capacities and molar volumes) of Li-bearing minerals, kaolinite, muscovite, diaspore and quartz.

| Minerals | $\Delta H_f^0$ (kJ mol$^{-1}$) | $\Delta G_f^0$ (kJ mol$^{-1}$) | $S^o$ (J K$^{-1}$ mol$^{-1}$) | $V$ (cm$^3$ mol$^{-1}$) | Cp = $a+bT+cT^{-2}$ $a^*$ (J K$^{-1}$ mol$^{-1}$) | $b\times10^3$* (J K$^{-2}$ mol$^{-1}$) | $c\times10^{-5}$* (J K mol$^{-1}$) |
|---|---|---|---|---|---|---|---|
| Eucryptite [1] | −2147.0 | −2027.24 | 84.85 | 47.97 | 108.11 | 87.76 | −17.68 |
| Spodumene [1] | −3053.0 | −2879.93 | 130.0 | 58.37 | 158.27 | 113.33 | −30.18 |
| Cookeite [1] | −8512.2 | −7888.67 | 504.8 | 196.2 | 534.31 | 376.95 | −124.93 |
| Petalite [1] | −4867.1 | −4591.25 | 233.2 | 128.4 | 258.65 | 164.43 | −55.15 |
| Muscovite [2] | −5981.63 | −5600.41 | 289.0 | 140.83 | 408.19 | 110.37 | −106.44 |
| Kaolinite [3] | −4118.16 | −3796.79 | 201.08 | 99.52 | 304.47 | 122.17 | −90.04 |
| Diaspore [4] | −999.80 | −921.26 | 35.34 | 17.76 | 46.94 | 6.41 | −11.3 |
| Microcline | 2600 | −3971.40 | −3746.24 | 213.93 | 108.741 | 320.566 | 18.03 |
| Quartz [2] | −910.7 | −856.33 | 41.5 | 22.69 | 43.18 | 40.67 | −9.62 |

[1] Vidal and Goffé (1991); [2] Johnson *et al.* (1992); [3] Zotov *et al.* (1998); [4] Khodakovsky and Westrum (1988)

reactions observed occur either in the kaolinite stability field (with small values of log ($a_{K^+}$) + pH) or in the muscovite stability field (with high values of log ($a_{K^+}$) + pH). Cookeite equilibrium cannot be achieved at a lower silica activity, whereas eucryptite and spodumene equilibria are impossible to attain.

In conclusion, the box defined by ($a_{Li^+}$) + pH, log ($a_{K^+}$) + pH, and log$(SiO_2)_{aq}$ appears to be the average composition of the hypothetical fluid in equilibrium with spodumene, cookeite and kaolinite in the temperature range 260−220ºC and pressure between 2.6 kbar and 2.2 kbar. It appears that in both stability diagrams, the lower limit of stability of cookeite is 205ºC and 2 kbar. This observation does not corroborate the conclusions of Vidal and Goffé (1991) who argued that cookeite is unstable below 260ºC, because they used a negative Gibbs free energy of formation of kaolinite ($\Delta G_f^0$ −3799.77 kJ mol$^{-1}$) from Berman (1988) and this value is more negative than the value used in this study. The K-feldspar stability (not represented in Figures 12 and 13) occurs for a high value of log ($a_{K^+}$) + pH, greater than 3.

## DISCUSSION

Lithium aluminosilicates (*e.g.* spodumene, petalite and eucryptite) are indicators of magmatic to subsolidus crystallization of Li-rich pegmatites (London and Burt, 1982). Many researchers suggest that spodumene may be altered either under hydrothermal or supergene conditions involving $Na^+/K^+$ or $H^+$ metasomatism and/or dissolution/crystallization processes. Alkaline metasomatism of spodumene involves the formation of albite, eucryptite + albite or muscovite + quartz assemblages

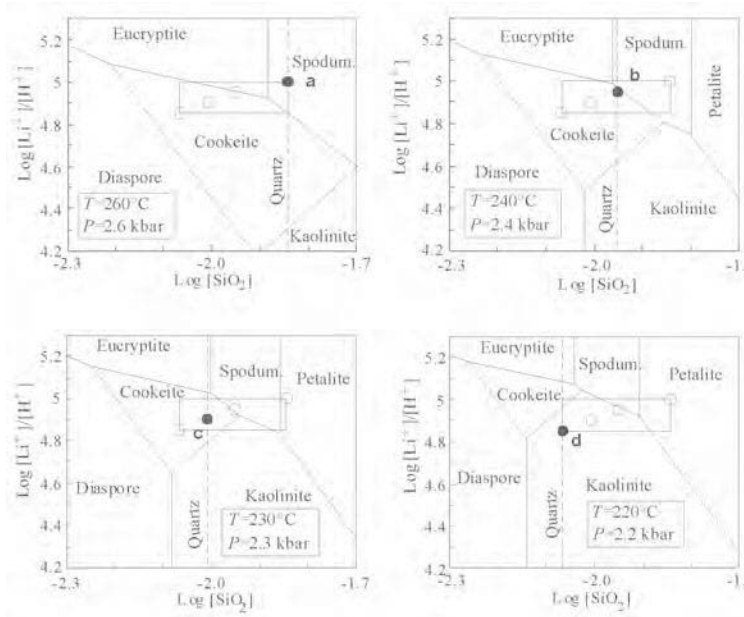


Figure 12. The diagram of log ($a_{Li^+}$) + pH *vs.* log ($a_{SiO_2}$) as a representation of the stability of cookeite.

https://doi.org/10.1346/CCMN.2007.0550306 Published online by Cambridge University Press

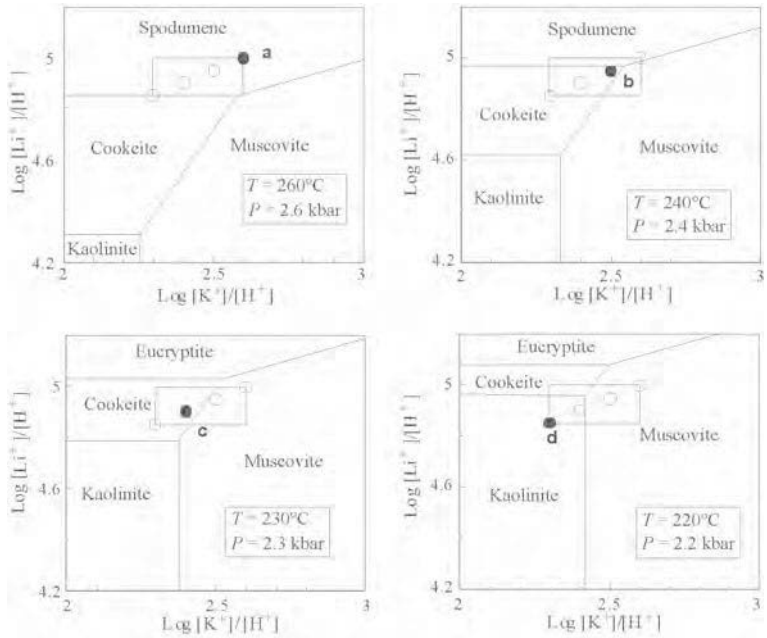


Figure 13. The diagram of log ($a_{Li^+}$) + pH *vs.* log ($a_{K^+}$) + pH as a representation of the stability of cookeite.

during the first stage of subsolidus alteration (London and Burt, 1982; Burt and London, 1982). Spodumene, petalite and eucryptite co-exist in the aplite-pegmatite dikes of northern Portugal. Here, both spodumene and petalite minerals were precipitated during a pegmatitic fluid phase, whereas both K-feldspar and eucryptite were formed from petalite alteration during alkaline metasomatism (Charoy *et al.*, 2001). Otherwise, albite and muscovite mainly replaced spodumene. Spodumene and petalite alteration to a mixture of eucryptite, albite, K-feldspar and white mica was interpreted as the normal consequence of re-equilibration in a restricted system (London and Burt, 1982; Wood and Williams-Jones, 1993).

Cookeite, the alteration product of spodumene, occurs associated with quartz or kaolinite ± mica. The petrography and chemiography of the cookeite + quartz and cookeite + kaolinite ± mica assemblages suggest a multiple phase hydrothermal evolution in the pegmatitic system. The cookeite + quartz assemblage occurs as micro-crack fillings in spodumene crystals (Figure 2a), suggesting that the spodumene dissolution rate was controlled by pH and pressure and temperature conditions. The direct alteration of spodumene to cookeite suggests an increase in $a_{H^+}$ in the pegmatitic system. This implies primary mineral dissolution and precipitation. We noted dissolution along the cleavage planes and flow dissolution of spodumene with the precipitation of a new layer phase (Figure 3b). Textural relationships between the two minerals are representative of nucleation and new mineral growth. Due to the drop in pH, high concentrations of Si and Al were required to develop and precipitate Al-rich clays. Consequently, the acid solutions dissolved spodumene, precipitated cookeite and liberated silica, according to the reaction:

$$\text{spodumene} + H^+ + H_2O = \text{cookeite} + SiO_2 \qquad (1)$$

The Al/Si ratio in cookeite suggests that its formation required a high Al activity. The excess Si went into solution precipitated as quartz, according to equation 1. The solubility and transport of Al is controlled by the alkali availability, and dissolution of minerals with Al/Li > 1 will lead to the formation of an Al-rich mineral phase (Anderson *et al.*, 1987). The relative Al enrichment is due to the preferential loss of other elements that are soluble in the uncomplexed form. Aluminum is a slightly mobile or immobile element (Carmichael, 1969), and mass-transfer studies assume that Al is conserved. The Al-constant frame postulated by Gresens (1971) means that all Al in the primary reactant minerals was recombined into the secondary minerals (*i.e.* cookeite). This conclusion is based on the assumption that the diffusion transport of Al was supplied from the spodumene through a virtually stagnant fluid, and the formation of significant amounts of cookeite has been regarded as evidence for very large fluid/rock ratios.

Alternatively, entire spodumene crystals were replaced by an assemblage of cookeite + kaolinite ± mica. Similarly, cookeite + 'hydromuscovite' assemblages associated with gold mineralization have previously been described in the literature (Brammal *et al.*, 1937). In fact, the cookeite ± mica assemblage is a non-isochemical reaction type for the spodumene alteration. Both clay phases form in a low-temperature environment, suggestive of metastable reactions. Spodumene replacement by mica is sometimes favored

https://doi.org/10.1346/CCMN.2007.0550306 Published online by Cambridge University Press

because the alteration reaction requires the addition of alkali cations and $H_2O$, where the available $K^+$ in the fluids results from the breakdown of K-feldspar. The susceptibility of aluminous silicates to alter into sheet silicates having the same Al/Si ratio was also reported for eucryptite-to-muscovite alteration where an Al/Si ratio of ~1 is maintained (London and Burt, 1982). Mica may form either directly from the alteration of cookeite or indirectly after cookeite has reacted to an intermediate phase as the fluid evolves and equilibrium is attained. Our back-scattered imaging observations reveal that the cookeite + kaolinite assemblage is surrounded by a matrix of mica grains, and no mica packets intergrown with cookeite were observed by TEM. This suggests that the mica was formed indirectly through an intermediary stage, after the cookeite + kaolinite assemblage formation.

The presence of kaolinite packets intergrown with cookeite packets was confirmed by both TEM and SAED. Significantly, kaolinite was found as a reaction product or as a by-product, probably in response to the low pH of the system. The Si/Al ratio and the temperature of the hydrothermal system played an important role in kaolinite formation. Normally, the Si/Al ratio lies close to unity for kaolinite crystallization. The formation of kaolinite is attributed to a decrease of pressure and temperature and a lower log ($a_{Li^+}$) + pH of the solutions. Thus, if the $a_{H^+}/a_{Li^+}$ is relatively high, the formation of kaolinite is favored. According to Eberl and Hower (1975), kaolinite may be synthesized at 150ºC and 5 bar, if the $a_{Li^+}/a_{H^+}$ ratio of the hydrothermal solution is small. By contrast, cookeite could crystallize from kaolinite if the $a_{Li^+}/a_{H^+}$ ratio is large, following interaction of Li-rich solutions with kaolinite. In the case discussed here, this did not happen.

The excess Al and silica needed for kaolinite precipitation are presumably supplied due to the slower reaction rate of cookeite formation. Usually, the Li enters into vacancies of the cookeite octahedral sheet, neutralizing the charge. However, when Li is hydrated, it is too large to enter into the octahedral sheet due to its envelope of hydrating water molecules, slowing the formation of cookeite layers. This assumption may be corroborated by the formation of kaolinite layers intergrown with cookeite. Thus, chemical solutions are heterogeneous, even at a scale of individual crystals, because of incongruent dissolution of crystals and very sluggish rates of homogenization of chemical systems at low temperatures (Lin and Clemency, 1981).

Textural and structural characteristics differentiated cookeite formed within spodumene cleavage fractures from cookeite formed as a replacement. The TEM images of cookeite (Figure 4) from fractures show direct crystallization from solutions in the pore spaces. Defects and dislocations in the (001) plane are more abundant in the cookeite specimens associated with quartz, being the result of both crystal growth processes and deformation (Bons, 1988). The stacking disorder should be caused by displacements of $b/3$, which take place both within the 2:1 layer and at the interlayer (Spinnler *et al.*, 1984).

The thickness of disordered 1L cookeite packets averaged ~85−100 nm. A disordered 2L polytype was observed in smaller cookeite packets with thicknesses of ~25 nm (Figure 6). Packets aligned and increased in size (Figure 9) when pseudomorphic replacement of spodumene became the dominant mechanism of cookeite formation. The SAED patterns revealed a high degree of layer disorder and a decreasing coherency in layer stacking of packets >450 nm (Figure 8, inset). The stacking sequences reflect metastable phases characterized by disordered polytypes commonly observed for low-grade pressure and temperature hydrothermal processes.

According to Jullien *et al.* (1996), cookeite polytypes from pegmatitic and metamorphic environments can be used as geobarometers. On the other hand, Mata *et al.* (2004) studied polytypism in cookeite in low-grade metapelites and found no correlation of well-ordered polytypes with pressure. The authors suggested that the cookeite series is an unlikely geobarometer because more than one stacking sequence is found in the same sample.

Thus, the pegmatitic cookeite samples analyzed by Jullien *et al.* (1996) were highly disordered in their stacking sequences. Nonetheless, the pegmatitic cookeite samples analyzed from northern Portugal confirm a structural evolution from disorder to 1L order-disorder with slightly disordered 2L intergrowths. Both 1L and 2L periodicities were found in the cookeite + quartz assemblage, where the lower limit of formation was estimated at 2.4 kbar and 240ºC. Crystallization at low temperatures tends to give rise to disordered or metastable phases. The rate and path of subsequent changes toward an equilibrium state are kinetically controlled by pressure, temperature, fluid composition and water/rock ratio. The most likely explanation lies in the apparently large differences in conditions at which disordered structures form. Also, Goffé *et al.* (1996) identified 1L cookeite coexisting with 3L cookeite or with highly disordered cookeite; mixing of these different types of structures suggests crystallization of cookeite during decompression from high- to low-grade metamorphic conditions. Otherwise, Schmidt and Livi (1999) suggested that temperature is a more important factor for trioctahedral chlorite polytypism than pressure and composition.

Chemical data for cookeite obtained by EMPA were compared with cookeite chemistry from both metamorphic and pegmatitic environments reported elsewhere. All investigated cookeite samples are closely grouped in the Li-Si-Al ternary diagram (Figure 9), where the progress of the reaction of spodumene to cookeite is measured by Al gain and Si loss.

In the total octahedral occupancy *vs.* $Li_2O$ (wt.%) diagram, both pegmatitic and metamorphic cookeite are

https://doi.org/10.1346/CCMN.2007.0550306 Published online by Cambridge University Press

plotted along the cookeite–donbassite joins. No confirmation of an intermediate continuous series from pegmatitic cookeite to sudoite has been found, as was described for metamorphic cookeite in Alpine metapelites by Goffé *et al.* (1996).

The pegmatitic cookeite series from northern Portugal ends half way along the cookeite–donbassite joins. Sample C5 (cookeite + quartz assemblage) is close to ideal cookeite, whereas C1 and C4 are plotted close to the field of metamorphic cookeite. This means no difference in octahedral cation content between metamorphic and pegmatitic cookeite. Cookeite samples C2 and C3 (cookeite + kaolinite assemblage) show an intermediate composition between donbassite and cookeite end-members, suggesting miscibility or a possible interstratification between di-trioctahedral and dioctahedral phases. Also, both pegmatitic and metamorphic cookeite are plotted along the cookeite–donbassite join in the $^{VI}$Al-(Mg + Fe)-Li ternary diagram.

Thus, Sudo (1978) proposed a possible intermediate cookeite–donbassite series which had also been reported elsewhere (Henmi and Yakamoto, 1965; Merceron *et al.*, 1989). Accordingly, the cookeite sample (C3) plotted along the cookeite–donbassite join corresponds to cookeite + kaolinite intergrowths. Therefore, the decrease in Li shows a considerable deviation of sample C3 towards the donbassite field, whereas both Si and Al remain constant due to the compositional contribution of kaolinite intergrown with cookeite.

The physicochemical conditions of both cookeite-bearing assemblages identified in pegmatite samples from northern Portugal now can be considered. It is interesting to compare our calculated activity ratios with the few experimentally determined concentration ratios in the literature. Wood and Williams-Jones (1993) showed that at low temperature and pressure conditions, $Li^+$ predominates over $K^+$ in aqueous solutions in equilibrium with Li aluminosilicates, alkali feldspars and quartz. Furthermore, $Li^+$ becomes more predominant with decreasing temperature. This suggests that if fluid chemistry changes from the K-feldspar to the spodumene-cookeite-muscovite field at 230ºC and ~2.3 kbar, the ratio will be very low, *i.e.* $\log K^+/Li^+ = 10^{-2}$. This means that the difference between $\log (a_{K^+})$ + pH and $\log (a_{Li^+})$ + pH is at least 2 units.

The pressure and temperature conditions for the emplacement of aplite-pegmatite dikes in northern Portugal exceeded 2.5 kbar and 450ºC (Charoy *et al.*, 2001). Spodumene is stable at pressures above 2 kbar in the petalite-eucryptite-quartz assemblage (London, 1984). The lowest limit of the spodumene to cookeite + quartz breakdown reaction was calculated at ~2.4 kbar and 240ºC (Figure 12). As implied by equation 1, this suggests that the pegmatitic system was saturated with respect to quartz. The equilibrium boundary of this reaction occurs through a large decrease of $\log(a_{Li^+})$ at constant pH or through an increase in the pH at constant $\log(a_{Li^+})$. The transformation of spodumene to cookeite is not possible when quartz equilibrium is close to the eucryptite-spodumene equilibrium. The pressure and temperature conditions of the divariant reaction cookeite + quartz = spodumene in the $Li_2O$-$Al_2O_3$-$SiO_2$-$H_2O$ system range from 280 to 450ºC and from 1 to 14 kbar (Vidal and Goffé, 1991). Accordingly, the cookeite + quartz assemblage coexists apparently in equilibrium at any given pressure, which obviously could be used as a geobarometer. Below the stability limit at ~2.4 kbar and 240ºC for the cookeite + quartz assemblage, cookeite may coexist in stability fields with other silicates, such as pyrophyllite, diaspore, kaolinite, mica, adularia and zeolites (Loughnan and Steggles, 1976; Foord *et al.*, 1986) in an advanced argillic alteration environment (Hemley and Johns, 1964). According to the literature, the formation conditions of cookeite in pegmatitic environments correspond to late deuteric stage (250–300ºC) or to secondary hydrothermal alteration of spodumene and petalite (Černý, 1970; Deshpande, 1978; Rikjs and Van der Vaen, 1972). However, the thermal stability field of cookeite in the Himalaya dike system (California) was evaluated by Foord *et al.* (1986) to be in the 350–400ºC range.

Spodumene-petalite-eucryptite coexist stably at ~2.2 kbar and 220ºC and at higher values of log $(a_{Li^+})$ + pH (Figure 12). It is noted that a fast decrease in log $(a_{Li^+})$ + pH and a slow input of $K^+$ in the pegmatitic system may favor mica formation, either directly from aluminous minerals or through intermediate steps (Cerný and Burt, 1991). The cookeite–mica equilibrium line (Figure 13) for different values of log $(a_{K^+})$ + pH is highly sensitive to decreasing pressure and temperature. Spodumene is completely replaced by cookeite at 2.2 kbar and 220ºC and the reactions observed in Figure 13 may occur either in the kaolinite stability field or in the muscovite stability field.

A possible mechanism for the mineralogical reactions observed at the nanometer scale in the Li-bearing aplite-pegmatite samples from northern Portugal is proposed in Figure 14. Two different scenarios for the alteration of spodumene to cookeite are pictured as a function of temperature and pressure conditions previously discussed where dissolution and precipitation processes have accompanied the mineralogical reaction.

## CONCLUSIONS

The alteration of spodumene to cookeite in the pegmatite district from northern Portugal is associated with two hydrothermal stages characterized by distinct pressure and temperature conditions. In a pegmatite environment, the mineral assemblages studied have an important petrological assignment: the cookeite and quartz assemblage may be associated with a greisen alteration related to the post-magmatic process of Li-bearing felsic rocks, whereas the cookeite and kaolinite

https://doi.org/10.1346/CCMN.2007.0550306 Published online by Cambridge University Press

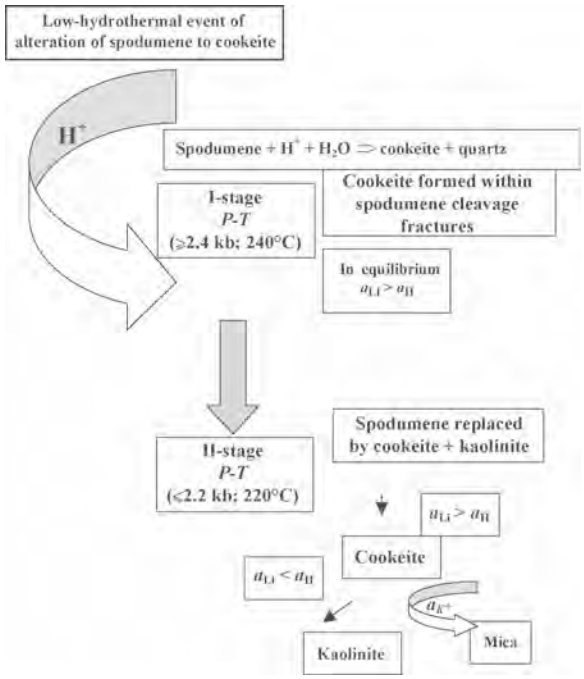


Figure 14. The mechanism of the alteration of spodumene to cookeite in the aplite-pegmatite field from northern Portugal.

assemblage corresponds to an argillic alteration stage. Dissolution of spodumene and cookeite precipitation directly from solutions in pore spaces is assumed to be the main alteration mechanism. In the first stage, cookeite precipitated in contact with an aqueous phase and in equilibrium with quartz. The sequence of cookeite crystallization involves a decrease of packet size as order increases and a change in chemical composition from cookeite end-members to an intermediate composition between cookeite and donbassite as order decreases. An evolution of the cookeite polytypism from fully disordered to semi-random 1L and 2L was identified. In the cookeite and quartz assemblage, the cookeite structure corresponds to a 1L order-disorder structure with a slight component of 2L disorder. Short-period 1L and 2L polytypes show an increasing amount of order with increasing pressure and temperature. Also, a high degree of disorder in the cookeite and kaolinite assemblage was observed. Nevertheless, the results obtained in this study and in that of Mata *et al.* (2004) confirm the presence of short-period intergrowths of 1L and 2L at low pressure, rather than at medium pressure, as assumed by Jullien *et al.* (1998).

The lower stability limit of the cookeite + quartz assemblage was calculated at ~2.4 kbar and 240ºC, and it corresponds with the observed assemblage breakdown. At ~2.2 kbar and 220ºC, spodumene is wholly replaced by the cookeite and kaolinite assemblage. The lower limit stability of cookeite corresponds to 205ºC and 2 kbar.

## ACKNOWLEDGMENTS

The authors are greatly indebted to Associate Editor Peter Heaney, to Dennis D. Eberl and to an anonymous reviewer for their helpful and constructive reviews. We are grateful to Olivier Vidal (Université 'J. Fourier' Grenoble, France) whose suggestions on early drafts of the manuscript greatly improved the thermodynamic section. Special thanks to M. M. Abad for technical help. R. Finkelman is also thanked for his help in improving the English.

## REFERENCES

Anderson, G.M., Pascal, M.L. and Rao, J. (1987) Aluminium speciation in metamorphic fluids. Pp. 297–321 in: *Chemical Transport in Metamorphic Processes* (H.C. Helgeson, editor). D. Reidel Publishing Company, Dordecht, The Netherlands.

Arsandaux, M.H. (1901) Sur quelques minéraux des environs de Brassac (Tarn, France). *Bulletin de la Société française de Minéralogie*, **24**, 428–432.

Bailey, S.W. and Lister, J.S. (1989) Structures, compositions and X-ray diffraction identification of dioctahedral chlorites. *Clays and Clay Minerals*, **37**, 193–202.

Berman, R.G. (1988) Internally consistent thermodynamic data for minerals in the system $Na_2O$-$K_2O$-CaO-MgO-FeO-$Fe_2O_3$-$Al_2O_3$-$SiO_2$-$TiO_2$-$H_2O$-$CO_2$. *Journal of Petrology*, **29**, 445–522.

Bons, A.J. (1988) Deformation of chlorite in naturally deformed low-grade rocks. *Tectonophysics*, **154**, 149–165.

Brammal, A., Leech, J.G.C. and Bannister, F.A. (1937) The paragenesis of cookeite and hydromuscovite associated with gold at Ogofan, Carmathenshire. *Mineralogical Magazine*, **24**, 507.

Brisbin, W.C. (1986) Mechanism of pegmatite intrusion. *American Mineralogist*, **71**, 644–651.

Burt, D.M. and London, D. (1982) Subsolidus equilibria. *Short Course Handbook*, **8**, pp. 329–346. Mineralogical Association of Canada, Quebec.

Carmichael, D.M. (1969) On the mechanism of prograde metamorphic reactions in quartz-bearing pelitic rocks. *Contributions to Mineralogy and Petrology*, **20**, 244–267.

Černý, P. (1970) Compositional variation in cookeite. *The Canadian Mineralogist*, **10**, 636–647.

Černý, P. (1972) The Tanco pegmatite at Bernic lake, Manitoba. Secondary minerals from the spodumene-rich zones. *The Canadian Mineralogist*, **11**, 660–678.

Černý, P. and Burt, D.M. (1991) Paragenesis, crystallochemical characteristics, and geochemical evolution of micas in granitic pegmatites. Pp. 257–297 in: *Micas* (P.H. Ribbe, editor). Reviews in Mineralogy, **13.** Mineralogical Society of America, Washington, D.C.

Černý, P., Povondra, P. and Stanek, J. (1971) Two cookeites from Czechoslovakia: a boron-rich variety and a II*b* polytype. *Lithos*, **4**, 7–15.

Charoy, B., Lhote, F., Dusausoy, Y. and Noronha, F. (1992) The crystal chemistry of spodumene in some granitic aplite-pegmatite of northern Portugal. *The Canadian Mineralogist*, **30**, 639–651.

Charoy, B., Noronha, F. and Lima, A. (2001) Spodumene-petalite-eucryptite mutual relationships and pattern of alteration in Li-rich aplite-pegmatite dikes from northern Portugal. *The Canadian Mineralogist*, **39**, 729–746.

Deshpande, M.L. (1978) Lithium resources in India. *Industrial Minerals*, **32**, 41–47.

Eberl, D. and Hower, J. (1975) Kaolinite synthesis: the role of the Si/Al and Alkali/$H^+$ ratio in hydrothermal systems. *Clays and Clay Minerals*, **23**, 301–309.

Ferreira, N., Iglésias, M., Noronha, F., Ribeiro, A. and Ribeiro,

M.L. (1987) Granitóides da zona Centro - Ibérica e seu enquadramento geodinâmico. Pp. 37–51 in: *Geologia dos los granitóides y rocas asociadas del Macizo Hesperico. Libro Homenaje a L.C. Garcia de Figuerola*, **1**. Editora Rueda, Madrid.

Fischer, G., Gibergy, P. and Glastre, P. (1989) Découverte de cookeite dans un filon à carbonates et sulfures du Dôme de la Mure (Isère, France). *Géologie des Alpes*, **65**, 39–44.

Flehmig, P.D. and Menschel, G. (1972) Über die lithiumgehalte und das Auftreten von cookeite (Lithium-chlorit) in Permischen sandsteinen von Nord-Hessen. *Contributions to Mineralogy and Petrology*, **34**, 211–223.

Foord, E.E., Starkey, H.C. and Taggart, J.E. (1986) Mineralogy and paragenesis of 'pocket' clays and associated minerals in complex granitic pegmatites, San Diego County, California. *American Mineralogist*, **71**, 428–439.

Goffé, B. (1977) Présence de cookéite dans les bauxites métamorphiques du Dogger de la Vanoise (Savoie). *Bulletin de la Société française de Minéralogie et Cristallographie*, **100**, 254–257.

Goffé, B., Baronnet, A. and Morin, G. (1994) La saliotite, interstratifié régulier 1:1 cookéite/paragonite: Un nouveau phyllosilicate du métamorphisme de haute pression et basse température. *European Journal of Mineralogy*, **6**, 897–911.

Goffé, B., Azañon, J.M., Bouybaouene, M.L. and Jullien, M. (1996) Metamorphic cookeite in Alpine metapelites from the Rif (Morocco) and Betic chain (Spain). *European Journal of Mineralogy*, **8**, 335–348.

Gresens, R.L. (1971) Application of hydrolysis to the genesis of pegmatite and kyanite deposits in northern New Mexico. *Mountain Geologist*, **8**, 3–16.

Heinrich, E.W. (1975) Economic geology and mineralogy of petalite and spodumene pegmatites. *Indian Journal Earth Sciences*, **2**, 18–29.

Hemley, J.J. and Johns, W.R. (1964) Chemical aspects of hydrothermal alteration with emphasis on hydrogen ion metasomatism. *Economic Geology*, **59**, 538–569.

Henmi, K. and Yamamato, T. (1965) Dioctahedral chlorite (sudoite) from Itaya, Okayama Prefecture, Japan. *Clay Science*, **2**, 92–101.

Hensen, B.J. (1967) Mineralogy and petrography of some tin, lithium and beryllium albite pegmatites near Doade, Galicia, Spain. *Leidse Geologische Mededelingen*, **39**, 249–259.

Ichikawa, A. and Shimoda, S. (1976) Tosudite from the Hokuno mine, Hokuno, Gifu Prefecture. *Clays and Clay Minerals*, **24**, 142–148.

Johnson, J.W., Oelkers, E.H. and Helgeson, H.C. (1992) *SUPCRT92:* A Software Package for Calculating the Standard Molal Thermodynamic Properties of Minerals, Gases, Aqueous Species, and Reactions from 1 to 5000 bars and 0º to 1000ºC. *Computers and Geosciences*, **18**, 899–947.

Julivert, M., Fontboté, J.M., Ribeiro, A. and Conde, L. (1974) Mapa tectónico de la Península Ibérica y Baleares. *Instituto Geológico Minero*, Madrid, Espanã, 114 pp.

Jullien, M., Baronnet, A. and Goffé, B. (1996) Ordering of the stacking sequence in cookeite with increasing pressure: An HRTEM study. *American Mineralogist*, **81**, 67–78.

Khodakovsky, I.L. and Westrum, E.F. (1988) Guidelines for International Geothermo-dynamics Tables. A set of Prototype Tables. *Codata Bulletin*, **7X**, 113 pp.

Lacroix, A. (1915) Manandonite et cookeite. *Bulletin de la Société française de Minéralogie et Cristallographie*, **38**, 142–149.

Lin, F.C. and Clemency, C.V. (1981) The kinetics of dissolution of muscovites at 25ºC and 1 atm $CO_2$, partial pressure. *Geochimica et Cosmochimica Acta*, **45**, 571–576.

London, D. (1984) Experimental phase equilibria in the system $LiAlSiO_4$-$SiO_2$-$H_2O$: a petrogenetic grid for lithium-rich pegmatites. *American Mineralogist*, **69**, 995–1004.

London, D. (1986) Formation of tourmaline-rich gem pockets in miarolitic pegmatites. *American Mineralogist*, **71**, 396–405.

London, D. and Burt, D.M. (1982) Alteration of spodumene and lithiophilite in pegmatites of the White Picacho district, Arizona. *American Mineralogist*, **67**, 97–113.

Loughnan, F.C. and Steggles, K.R. (1976) Cookeite and diaspore of the Back Creek pyrophyllite deposit near Pambula, N-Wales. *Mineralogical Magazine*, **40**, 765–772.

Mata, P., Peacor, D.R. and López-Aguayo, F. (2004) Polytypism of cookeite in low-grade metapelites of the Cameros Basin, Spain: Lack of correlation of well ordered polytypes with pressure. *American Mineralogist*, **89**, 1510–1515.

Merceron, T., Inoue, A., Bouchet, A. and Meunier, A. (1989) Lithium bearing donbassite and tosudite from Echasières, Massif Central, France. *Clays and Clay Minerals*, **36**, 39–46.

Miser, H.D. and Milton, C. (1964) Quartz, rectorite and cookeite of the Jeffrey Quarry, near North Little Rock, Arkansas. *Arkansas Geological Commission Bulletin*, **21**, 29 pp.

Noronha, F., Ramos, J.M.F., Rebelo, J., Ribeiro, A. and Ribeiro, M.L. (1981) Essai de corrélation des phases de déformation hercyniennes dans le NW de la Péninsule Ibérique. *Leidse Geologische Mededelingen*, **52**, 1, 87–91.

Orliac, M., Permingeat, F., Tollon, F. and Passaqui, B. (1971) Cookeite dans des felons de quartz des Pyrénées centrals (Ariege et Haute-Garonne). *Bulletin Société française de Minéralogie et Cristallographie*, **94**, 396–401.

Pecora, W.T., Switzer, G., Barbosa, A.L. and Myers, A.T. (1950) Mineralogy of the Golgonda pegmatite, Minas Gerais, Brazil. *American Mineralogist*, **35**, 889–901.

Penfield, S.L. (1894) On cookeite from Paris and Hebron, Maine. *Bulletin de la Société française de Minéralogie et Cristallographie*, **17**, 223–224.

Quensel, P. (1937) Minerals of the Varuträsk pegmatite. VI. On the occurrence of cookeite. *Geologiska Föreningens i Stockholm Förhandlingar*, **59**, 262.

Quensel, P. (1956) The paragenesis of the Varuträsk pegmatite including a review of its mineral assemblage. *Arkiv för Mineralogi och Geologi*, **2**, 9–126.

Ren, S.K., Eggleton, R.A. and Walshe, J.L. (1988) The formation of thermal cookeite in the breccia pipes of the Ardletha New South Wales, Australia. *The Canadian Mineralogist*, **26**, 407–421.

Rikjs, H.R.P. and Van Der Veen, A.H. (1972) The geology of tin-bearing pegmatites of the eastern part of Kamitivi district, Rhodesia. *Mineralium Deposita*, **7**, 385–395.

Sahama, T.G., Knorring, O.V. and Lehtinen, M. (1968) Cookeite from the pegmatite, Zambezia, Mozambique. *Lithos*, **1**, 12–19.

Sartori, M. (1988) L'unite du Barrhorn (zone Pennique, Valais, Suisse). PhD thesis, Université de Lausanne, Switzerland, 150 pp.

Schmidt, D. and Livi, J.T. (1999) HRTEM and SAED investigations of polytypism, stacking disorder, crystal growth, and vacancies in chlorites from subgreenschist facies outcrops. *American Mineralogist*, **84**, 160–170.

Shimada, N., Kusachi, I. and Sugaki, A. (1985) Cookeite from antimony veins of the Cracatoa mines. *Mineralogical Journal*, **12**, 218–224.

Singh, B. and Gilkes, R.J. (1993) Weathering of spodumene to smectite in a lateritic environment. *Clays and Clay Minerals*, **41**, 624–630.

Spinnler, G.E., Self, P.G., Iijima, S. and Buseck, P.R. (1984) Stacking disorder in clinochlore chlorite. *American Mineralogist*, **69**, 256–263.

Stone, C.G. and Milton, C. (1976) Lithium mineralization in Little Rock, Arkansas. *US Geological Survey Professional Paper*, **1005**, 137–142.

Sudo, T. (1978) An outline of clays and clay minerals in Japan. Pp. 1–103 in: *Clays and Clay Minerals in Japan* (T. Sudo and M. Shimoda, editors). *Developments in Sedimentology*, **26**, Elsevier, Amsterdam.

Theye, T., Seidel, E. and Vidal, O. (1992) Carpholite, sudoite and chloritoid in low-temperature, high-pressure metapelites from Crete and the Peloponnese, Greece. *European Journal of Mineralogy*, **4**, 487–507.

Velde, B. (1984) Electron microprobe analysis of clay minerals. *Clay Minerals*, **19**, 243–247.

Vidal, O. and Goffé, B. (1991) Cookeite experimental study and thermodynamic analysis of its compatibility relations in the $Li_2O$-$Al_2O_3$-$SiO_2$-$H_2O$ system. *Contributions to Mineralogy and Petrology*, **108**, 72–81.

Wood, S.A. and Williams-Johns, A.E. (1993) Theoretical studies of the alteration of spodumene, petalite, eucryptite and pollucite in granitic pegmatites: exchange reactions with alkali feldspars. *Contributions to Mineralogy and Petrology*, **114**, 255–263.

Zagorsky, V.Y., Peretyazhko, I.S., Sapozhnikov, N.A., Zhukhlistov, A.P. and Zvyagin, B.B. (2003) Borocookeite, a new member of the chlorite group from the Malkhan gem tourmaline deposits, Central Transbaikalia, Russia. *American Mineralogist*, **88**, 830–836.

Zotov, A., Mukhametgaleev, A. and Schott, J. (1998) An experimental study of kaolinite and dickite relative stability at 150–300ºC and the thermodynamic properties of dickite. *American Mineralogist*, **83**, 516–524.

(*Received 14 March 2005; revised 18 January 2007; Ms. 1027; A.E. Peter J. Heaney*)